Bull. Mater. Sci., Vol. 35, No. 7, December 2012, pp. 1079–1085. © Indian Academy of Sciences.

Chemically ordered face-centred tetragonal Fe–Pt nanoparticles embedded SiO_2 films

SOURAV PRAMANIK and GOUTAM DE*
Nano-Structured Materials Division, Central Glass and Ceramic Research Institute, Kolkata 700 032, India

MS received 21 February 2012

Abstract. **Chemically ordered face-centred tetragonal (fct) Fe–Pt alloy nanoparticles (NPs) embedded SiO_2 films were synthesized on glass substrate by *in situ* hybrid sol–gel approach followed by heating at 450–900 °C in air and reducing (10% H_2–90% Ar) atmospheres. Heat treatment of Fe/Pt co-doped films in air caused generation of Pt NPs first. At this stage, Fe remained in ionic state covalently bonded with silica network. Further heat treatment at 800–900 °C in reducing atmosphere facilitated the formation of uniformly dispersed fct Fe–Pt alloy NPs in amorphous SiO_2 film matrix. The generated alloy composition was estimated by grazing incidence X-ray diffraction and TEM analysis to be $Fe_{0.42}Pt_{0.58}$ which is close to the nominal value.**

Keywords. **fct Fe–Pt alloy nanoparticles; Pt nanoparticles; sol–gel SiO_2 films embedded with nanoparticles; nanocomposite films.**

1. Introduction

Magnetic nanoparticles (NPs) can be broadly classified into three different classes, viz. metal oxides, metal alloys and metallic NPs. Metal oxides which are quite stable under ambient conditions, do not exhibit very strong magnetic properties. Conversely, metallic NPs are magnetically strong but unstable due to oxidation in ambient condition. Among the magnetic alloy NPs, face-centred tetragonal (fct) Fe–Pt NPs has important applications in high density storage devices (Sun *et al* 2000; Zeng *et al* 2002; Sun 2006; Wang *et al* 2009; Kong *et al* 2011). It is known that a chemically disordered face-centred cubic (*fcc*) phase has been usually formed in case of as-synthesized Fe–Pt alloy NPs at low temperature and the structure is transformed to chemically ordered fct structure (known as $L1_0$) after annealing at high temperature (Sun *et al* 2000; Lu *et al* 2004; Howard *et al* 2005; Wang *et al* 2009). The chemically ordered Fe–Pt alloys are very important because of their large uniaxial magnetocrystalline anisotropy and good stability, whereas disordered *fcc* phase has very small coercivity and soft magnetic properties at room temperature (Sun *et al* 2000; Howard *et al* 2005; Wang *et al* 2009). The size and shape dependent magnetic properties of Fe–Pt alloy NPs in fabricating new magnetic devices (Wellons *et al* 2007; Chou *et al* 2009) are also noteworthy. Besides magnetic applications, Fe–Pt alloy NPs has also important applications in catalysis (Watanabe *et al* 2000; Igarashi *et al* 2001; Chen *et al* 2006, 2007a,b). It was observed that Fe–Pt alloy NPs showed excellent tolerance towards CO poisoning in formic acid electro-oxidation (Chen *et al* 2006, 2007a,b).

Keeping in view different important applications, in a series of work, we have showed fabrication of several metal alloy NPs incorporated dielectric films with controlled alloy using a simple sol–gel chemical process (De and Rao 2003, 2005; Mattei *et al* 2002; Kiran *et al* 2004; Pal and De 2005, 2007, 2008; Jana *et al* 2009; Pramanik *et al* 2011). In this paper we describe the synthesis of Fe–Pt alloy NPs incorporated SiO_2 films using the *in situ* inorganic–organic hybrid sol–gel approach followed by thermal treatments. The films and the embedded Fe–Pt NPs were characterized by UV-visible spectroscopy, spectroscopic ellipsometry, grazing incidence X-ray diffraction studies and transmission electron microscopy.

2. Experimental

2.1 *Materials*

All chemicals were used as received. Tetraethyl orthosilicate (TEOS), 3-(glycidoxypropyl) trimethoxysilane (GLYMO) and $FeCl_3$ were supplied by Sigma-Aldrich, while, $H_2PtCl_6{\cdot}6H_2O$, *n*-butanol and methanol were obtained from S.D. Fine Chem. Limited. Aluminum acetylacetonate ($Al(acac)_3$) was supplied by Lancaster.

2.2 *Sol preparation*

The detailed preparation techniques of the inorganic–organic hybrid sols using tetraethyl orthosilicate (TEOS) and 3-(glycidoxypropyl) trimethoxysilane (GLYMO) and coatings were described elsewhere (Pal and De 2005; Medda and De 2009). Briefly, TEOS and GLYMO (2·3:1 mol ratio) were

*Author for correspondence (gde@cgcri.res.in)

dissolved in *n*-butanol (65 wt% of the total). This mixed alkoxide solution was hydrolyzed using a mixture of water and HCl (0·5 and 5×10^{-4} mol/mol of alkoxy group, respectively). Then the resultant mixture was refluxed for 60 min and a catalytic amount of Al(*acac*)$_3$ was added at this stage with stirring followed by mixing of the remaining *n*-butanol (35%). The resulting clear sol was used for doping.

2.3 *Metal ion doping*

In case of individual metal doping, metal salt (Fe or Pt) was doped into the hybrid silica sol keeping the molar ratio of metal (Fe or Pt) and equivalent SiO_2 of 5:95. For Fe–Pt system, a molar ratio of Fe:Pt:SiO_2 = 5:5:90 was maintained. In the final sol, about 8 equivalent wt% of SiO_2 was maintained in all cases. To prepare the doped sols, required amounts of metal salts were dissolved in water (the molar ratio of water to salt can be varied from 26 to 28) and mixed with the inorganic–organic hybrid silica sol while stirring. After stirring for about 30 min, the doped sols were used for film deposition. The nominal composition of the sols is given in table 1.

2.4 *Preparation of films*

Prior to the coating deposition, silica glass slides (Heraus, Suprasil 3; thickness 0·5 mm) were first cleaned with a warm neutral detergent solution, followed by rinsing with distilled water and 2-propanol, and finally, boiled in 2-propanol for 5 min. The coatings were prepared using the dipping technique (Dip-master 200, Chemat Corporation) with a withdrawal velocity of 8 in min^{-1}. The coated films were first dried at 60 °C for 1 h and then subjected to heat treatment at 450 °C (ramp 2 deg min^{-1}) in air for 1 h to remove the organics. The films were then heated (ramp 2 deg min^{-1}) in 10%H_2–90%Ar (H_2–Ar) atmosphere at 800 and 900 °C with a holding time of 1 h at the respective temperatures to facilitate alloy formation. All heat treatments were done in a cumulative heating procedure. Undoped matrix films were also prepared on one side polished Si wafer and heat treated in similar way as those of doped films for refractive index measurement.

Table 1. Nominal compositions of the sols.

Sample	Nominal equivalent molar ratio		Expected metal NPs to be formed inside SiO_2 film
	Components	Molar ratio	
Fe/SiO_2	Fe:SiO_2	5:95	Fe
Pt/SiO_2	Pt:SiO_2	5:95	Pt
Fe–Pt/SiO_2	Fe:Pt:SiO_2	5:5:90	$Fe_{0.5}Pt_{0.5}$

2.5 *Film characterization*

The UV-vis spectra of the heat treated films deposited on silica glass substrates were recorded using a Cary 50 scan spectrophotometer. Grazing incidence X-ray diffraction (GIXRD) patterns of the coatings deposited on silica glass substrates were recorded using Rigaku SmartLab (operating at 9 kW using the rotating anode and cross-beam optics to enhance the X-ray intensity). A grazing incidence angle of the X-ray was maintained at 0·3° for all analysed film samples. TEM was performed using a Tecnai G^2 30ST (FEI company) operating at 300 kV. TEM samples were prepared by scraping the heat-treated films deposited on silica glass substrate. The scraped films were first dispersed in methanol under ultrasonication, and one small drop of this dispersion was placed onto a carbon-coated grid. Refractive index and thickness of the undoped and doped films were measured using a spectroscopic (400–1000 nm) ellipsometer (J. A. Woollam Co., Inc.; model M2000). In case of Fe, Pt and Fe–Pt doped (absorbing in the visible region) films, the thickness values were evaluated ellipsometrically by fitting the refractive index and extinction coefficient curves in the non-absorbing region (800–1000 nm). In all cases the ellipsometric measurements were done in at least 3 different places of the films to check the homogeneity.

3. Results and discussion

3.1 *Optical and ellipsometric characterization*

The inorganic–organic hybrid approach has been used to obtain crack or spot-free, relatively thicker SiO_2 films on glass substrates after heat treatment. The adhesion and hardness of the heat-treated films were also found to be excellent. All as-prepared films were visually transparent and crack-free. After heat treatment in air at 450 °C, the Fe-doped films remained colourless whereas Pt- and Fe–Pt-doped films became brownish. On further heat treatment in H_2-Ar atmosphere the films remained transparent and crack-free but became light brownish (Fe) to brownish (Pt and Fe–Pt) in colour. Representative optical spectra of Fe, Pt and Fe–Pt doped films heat-treated at 800 °C in H_2-Ar are shown in figure 1. The spectrum of similarly prepared and heat-treated matrix SiO_2 film (undoped) is also shown in figure 1. As shown in the figure the spectra of the heat-treated Fe, Pt and Fe–Pt doped films absorb continuously in the visible to UV region due to light scattering (Creighton and Eadon 1991). In case of Fe–Pt, the absorbance value is higher because of higher concentration of metallic NPs and alloy formation (table 1). The films were also characterized ellipsometrically to evaluate film thickness and refractive index values. The undoped matrix SiO_2 film heat-treated at 800 °C is almost non-absorbing showing the k value close to 0 and refractive index values in the range of 1·442–1·425 in the wavelength region 400–1000 nm region (figure 2a). Such ellipsometric measurement of the undoped film gave a thickness value of 319 nm. It can be noted here that the refractive index

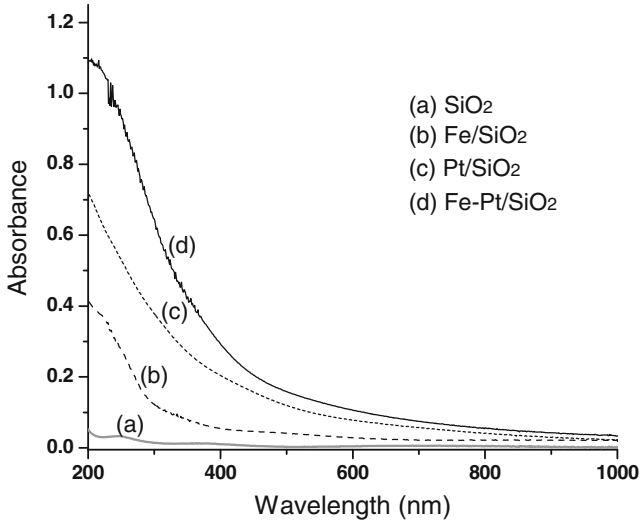

Figure 1. UV–Vis spectra of (a) undoped SiO_2 film and (b) Fe, (c) Pt and (d) Fe–Pt alloy NPs incorporated SiO_2 films heat-treated at 800 °C in H_2–Ar.

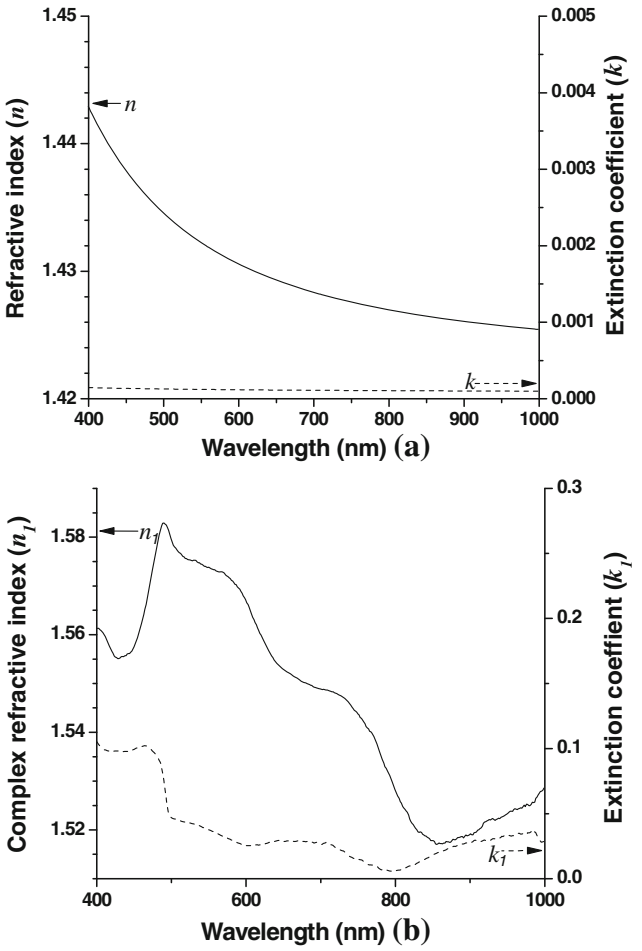

Figure 2. Refractive index and extinction coefficient curves of (**a**) undoped SiO_2 film and (**b**) Fe–Pt alloy NPs doped SiO_2 film annealed at 800 °C in H_2–Ar. The measurement was done using a spectroscopic ellipsometer.

(n) value of undoped film is slightly lower compared to the dense amorphous SiO_2 (1·475–1·455). Such a difference in n value indicates presence of ∼6% porosity (volume % porosity) in the matrix SiO_2 film synthesized in the present study. The porosity has been generated due to the inorganic–organic hybrid synthetic protocol used, as also observed previously (Pal and De 2008, 2009). Since the doped films absorbed from about 800 nm onwards they showed large extinction (k_1) and complex refractive index (n_1) values. For this purpose the thickness values of these films were evaluated ellipsometrically by fitting n_1, k_1 curves in the non-absorbing region (800–1000 nm). The ellipsometric results of the representative Fe–Pt alloy NPs doped SiO_2 film heat-treated at 800 °C is shown in figure 2b. As shown in this figure the film showed low k_1 values in the range of 800–1000 nm (figure 2b, dashed curve). The film thickness values of the Fe, Pt and Fe–Pt NPs doped films heat-treated at 800 °C were estimated to be 325, 321 and 338 nm, respectively by such ellipsometric measurements. The amount of porosity of doped films could not be evaluated directly by ellipsometric measurements. However, as the similarly heat-treated undoped films showed a porosity of ∼6%, the doped films are also expected to be slightly porous in nature.

3.2 *GIXRD studies*

GIXRD of Fe, Pt and Fe–Pt-doped films heat-treated at different temperatures were studied to observe the evolution of embedded NPs in SiO_2 film matrix and their structure. GIXRD of Fe-doped SiO_2 (figure 3a) film heat-treated at 450 °C in air shows typically an amorphous SiO_2 like pattern showing no Fe related diffraction peaks. It can be assumed that Fe remains in this film in ionic state since Fe can form polymeric chains like –O–Si–O–Fe–O–Si–O– occupying the tetrahedral sites of silica network (Jitianu *et al* 2002). The –O–Si–O–Fe–O– bonding was quiet stable and even at 800 °C in H_2–Ar (reducing) atmosphere a very little amount of iron was found to be reduced with the formation of Fe NPs (a small Fe metal peak is observed in figure 3a, curve 2) and most of the iron remained as iron ions covalently bonded with the silica network. Further heat treatment at 900 °C in H_2–Ar caused crystallization of silica matrix to mainly tetragonal cristobalite (JCPDS no. 01-089-7194) phase. Figure 3a (curve 3) shows presence of a very strong peak at 21·8° 2θ and other Bragg reflections corresponding to the cristobalite SiO_2 along with possibly a small Fe metal peak (marked with red line) overlapped with cristobalite peak. It is known that the presence of Fe^{2+} or Fe^{3+} individually does not influence the crystallization of silica even at high temperature. However, co-existence of Fe^{2+}/Fe^{3+} ions induced the crystallization process (Guglielme and Maschio 1985; Nanri *et al* 1996). In the present system, during the reduction process (in H_2-Ar atmosphere) of the doped Fe^{3+} ions at elevated temperature (900 °C), a Fe^{3+}/Fe^{2+} mixture (part

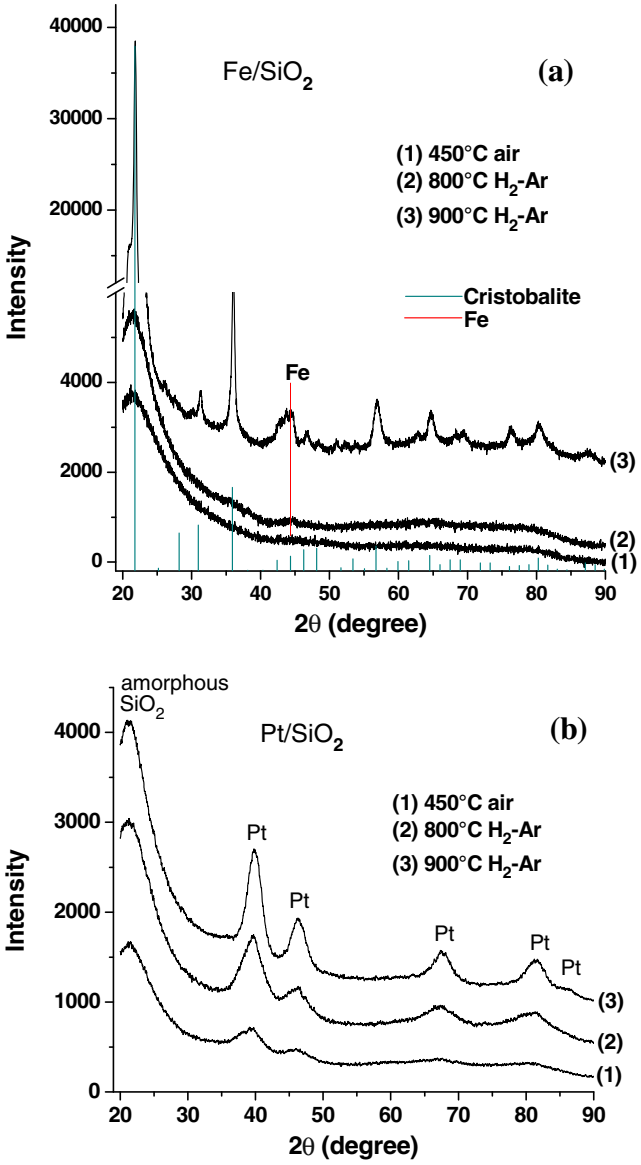

Figure 3. GIXRD patterns of (**a**) Fe and (**b**) Pt-doped SiO_2 films annealed at different temperatures. In (**a**) cristobalite SiO_2 and Fe peaks are indicated by deep cyan and red lines, respectively. Annealing temperatures are indicated in body of figure. *Y*-axis scales are shifted for clarity.

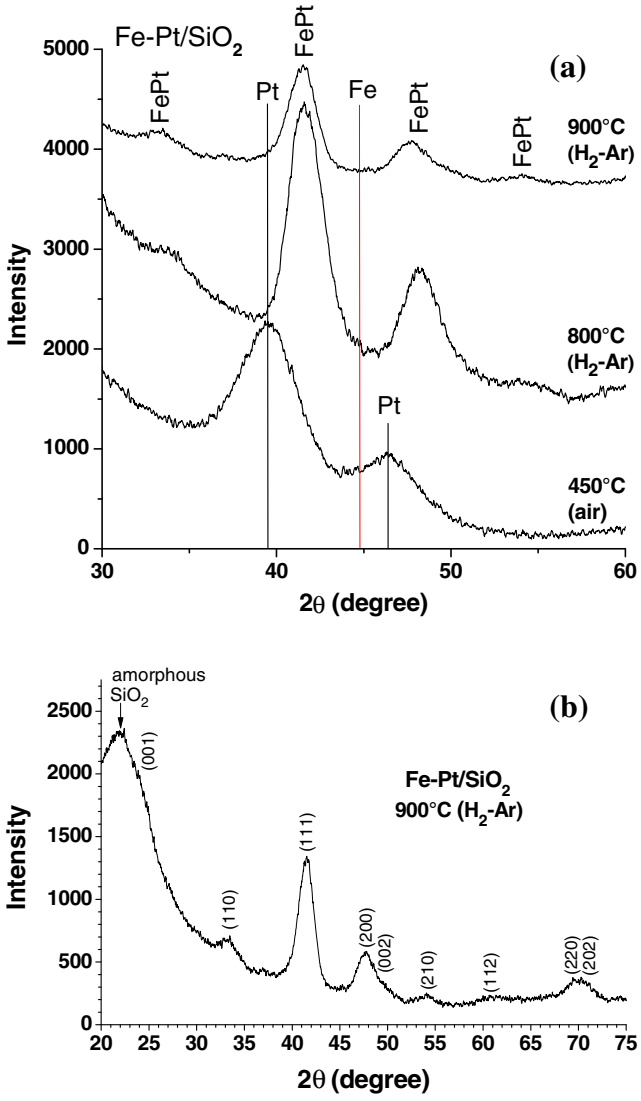

Figure 4. (**a**) GIXRD patterns showing evolution of Fe–Pt-doped silica films annealed at different temperatures and (**b**) diffraction pattern of 900 °C annealed film covering range from 2θ = 20 to 75°. In (**a**) fct Fe–Pt peaks are labelled as FePt and positions of Pt and Fe peaks are indicated by black and red lines, respectively. In (**b**) all fct Fe–Pt alloy related peaks are indicated by respective crystallographic planes (*hkl*). In case of (**a**) Y-axis scales are shifted for clarity.

reduction of $Fe^{3+} \rightarrow Fe^{2+}$) would be expected to be formed first. During such transformation, a rearrangement in the silica network containing Fe (–O–Si–O–Fe–O–) took place leading to crystallization.

GIXRD of Pt-doped films (figure 3b) showed characteristic diffraction peaks due to the *fcc* platinum (JCPDS no. 01-087-0636) in all the heat-treated films. It has been observed that the Pt NPs of size 3·1 nm are formed at 450 °C in air and with further heat treatment in H_2–Ar at 800 and 900 °C, the size of Pt NPs increased to 4 and 4·3 nm, respectively. Average crystallite size of the Pt NPs was estimated from the X-ray line broadening using Scherrer formula. The silica matrix remains amorphous for all the heat-treated Pt-doped films. This is because the inert metallic Pt NPs were formed at the early stage (450 °C) and remain embedded in the amorphous silica film matrix.

GIXRD patterns of Fe–Pt doped films heat-treated at different temperatures are presented in figure 4. In case of 450 °C (air) annealed film only Pt related peaks are observed confirming that the Fe remains in the matrix as ionic form. The size of the Pt NPs remained similar as observed in case of only Pt-doped films. When this film was further heat-treated at 800 °C in reducing atmosphere, Fe–Pt alloy NPs are generated and GIXRD pattern (figure 4b, curve 2) showed Bragg diffractions corresponding to the fct Fe–Pt

alloy. Interestingly in case of only Fe-doped films, at 800 °C, formation of Fe NPs was inhibited whereas in presence of Pt, Fe easily entered into the Pt lattice. In this case no individual Fe metal related peak was observed (see position of main Fe metal peak shown in figure 4b by red line), and all Fe ions were reduced to Fe metal and formed solid solution with Pt. The alloy composition of the embedded fct Fe–Pt alloy NPs was calculated from the lattice parameters (a) obtained from GIXRD (Pramanik *et al* 2011) using the Vegard's law which is found to be $Fe_{0.424}Pt_{0.576}$. The estimated alloy composition is close to the nominal value (see table 1). Further increase of temperature to 900 °C showed slight increase of crystallite size of fct Fe–Pt alloy NPs, however, the lattice parameter as well as alloy composition remained similar. More interestingly, as almost all Fe formed solid solution with Pt, the matrix SiO_2 remained amorphous because of the absence of Fe ions in the matrix which favoured crystallization of SiO_2. The average crystallite size of the embedded fct Fe–Pt alloy NPs in the 800 and 900 °C heat-treated films was estimated to be 4·4 and 5·1 nm, respectively.

3.3 *TEM studies*

The structure, distribution and composition of fct Fe–Pt alloy NPs embedded in the silica film were analysed by a TEM operating at 300 kV attached with an energy

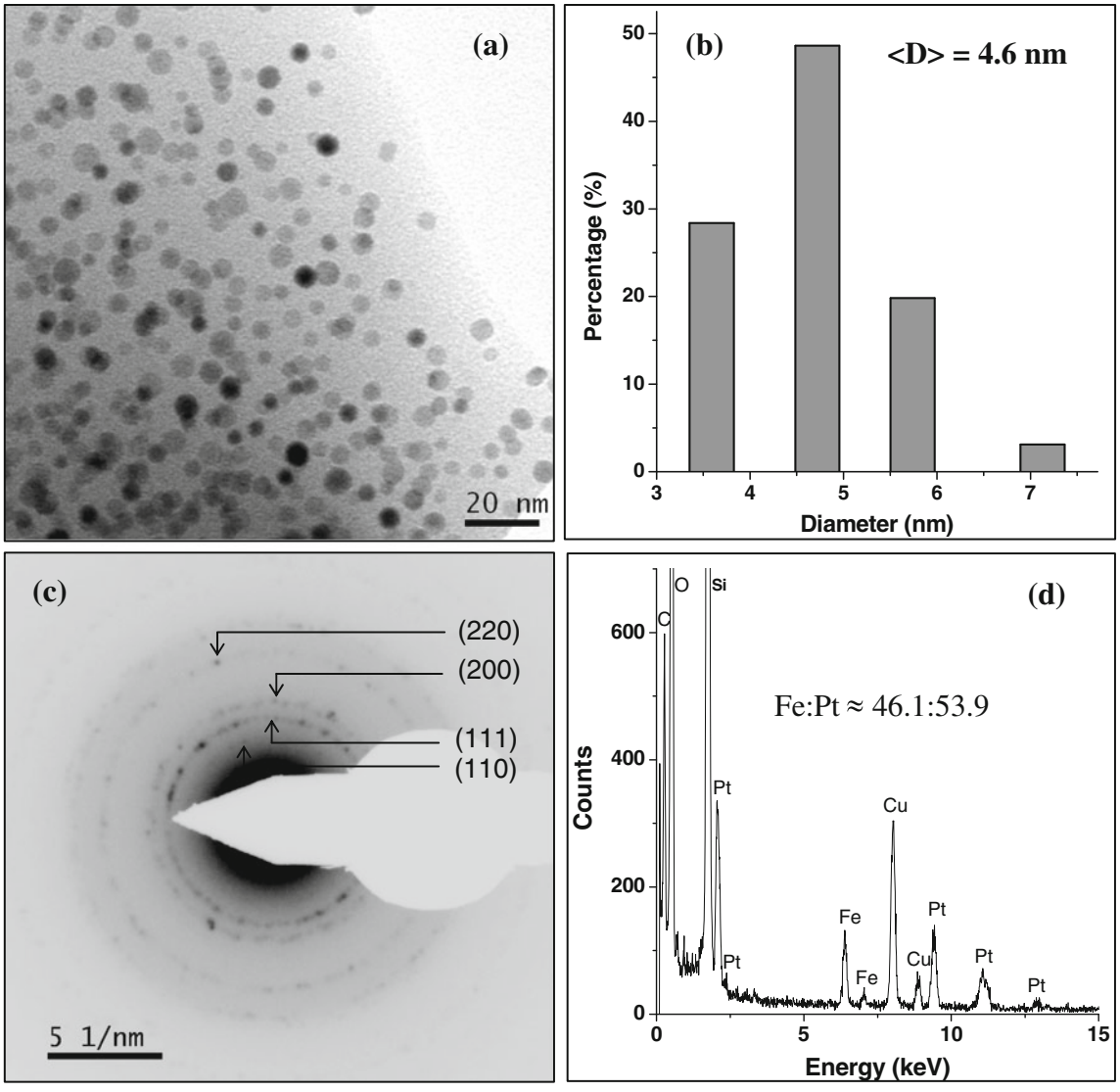

Figure 5. Transmission electron microscopy (TEM) images of Fe–Pt-doped SiO_2 film annealed at 800 °C in H_2–Ar: (**a**) bright field TEM image showing Fe–Pt bimetallic alloy NPs embedded in SiO_2 film matrix, (**b**) histogram showing size distribution of Fe–Pt alloy NPs obtained from bright field TEM image, (**c**) corresponding SAED pattern and (**d**) energy dispersive X-ray analysis (EDX) spectrum taken from bright field image. Cu signals observed in EDX pattern are from Cu grid.

dispersive X-ray analysis (EDX) system. Figure 5 represents TEM results of the representative sample heat-treated at 800 °C in H_2–Ar atmosphere. The low resolution bright field image (figure 5a) shows the presence of uniformly dispersed Fe–Pt NPs of average size, 4·6 nm, which is well in agreement with the result obtained from GIXRD. The selected area electron diffraction (SAED) pattern (grey scale inverted; figure 5c) obtained from the region shown in the bright field TEM micrograph shows the diffraction rings corresponding to the d-values of 0·260, 0·218, 0·190 and 0·135 nm originating from the (110), (111), (200) and (220) lattice planes, respectively. These d-values are in agreement with the fct $Fe_{0·42}Pt_{0·58}$ alloy as also observed by GIXRD. The average lattice parameter (a) estimated from the d-values in the SAED pattern (0·377 nm) was also matching with the value obtained in GIXRD (0·375 nm). This result confirmed that the alloy composition (fct $Fe_{0·42}Pt_{0·58}$) is well maintained in the film. The atomic ratios of Fe–Pt in the film was checked using energy dispersive X-ray analysis (EDX). One representative EDX spectrum obtained from the region in the bright field image is shown in figure 5d. Such spectrum showed the presence of Si, O, Fe and Pt. The peaks of C and Cu were from carbon coated Cu grids used for TEM studies. Quantitative EDX analysis gave an average Fe : Pt atomic ratio of 0·46:0·54 which is close to the nominal Fe/Pt atomic ratio (table 1) and the alloy composition obtained from the lattice parameter values.

The fct Fe–Pt alloy NPs were also analysed by high resolution TEM (HRTEM). Figure 6 shows HRTEM image of such alloy NPs. Presence of Fe–Pt lattice fringe patterns is clearly visible in the HRTEM image (see also the inset of figure 6).

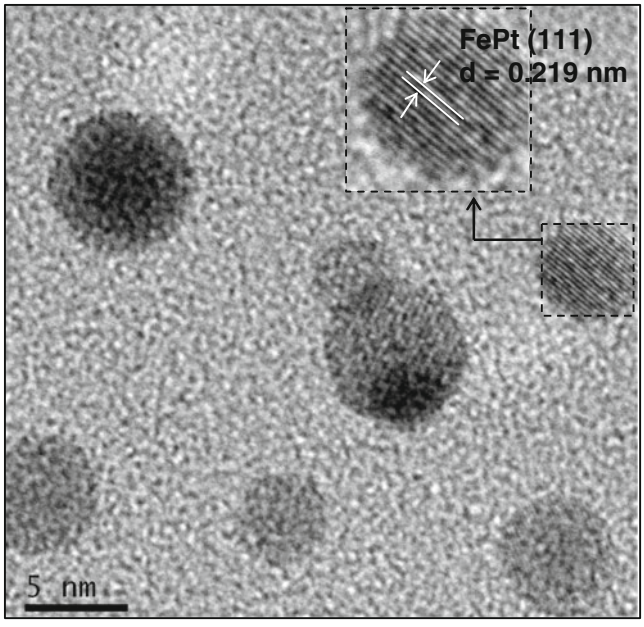

Figure 6. High-resolution TEM image showing Fe–Pt (111) crystalline planes corresponding to alloy NP. Inset shows magnified view of one NP with labelling.

The d-value calculated from the lattice spacing is found to be 0·219 nm (d_{111}), and this value matches with the alloy composition ($Fe_{0·42}Pt_{0·58}$) as also estimated from the GIXRD and SAED patterns.

The compositional homogeneity of the embedded alloy NPs was also checked by the high-angle annular dark-field (HAADF) imaging technique in scanning TEM (STEM) mode. The HAADF–STEM image of the alloy NPs is shown in figure 7a. To estimate the Fe–Pt alloy composition EDX measurement was performed using the nano-probe in STEM mode on single NPs. For this purpose a few NPs were chosen arbitrarily and marked as 1–5 in figure 7a with red dashed circles where nano-probes were focused. All the analysed individual particles showed signals of Fe and Pt with similar composition confirming the formation of uniform

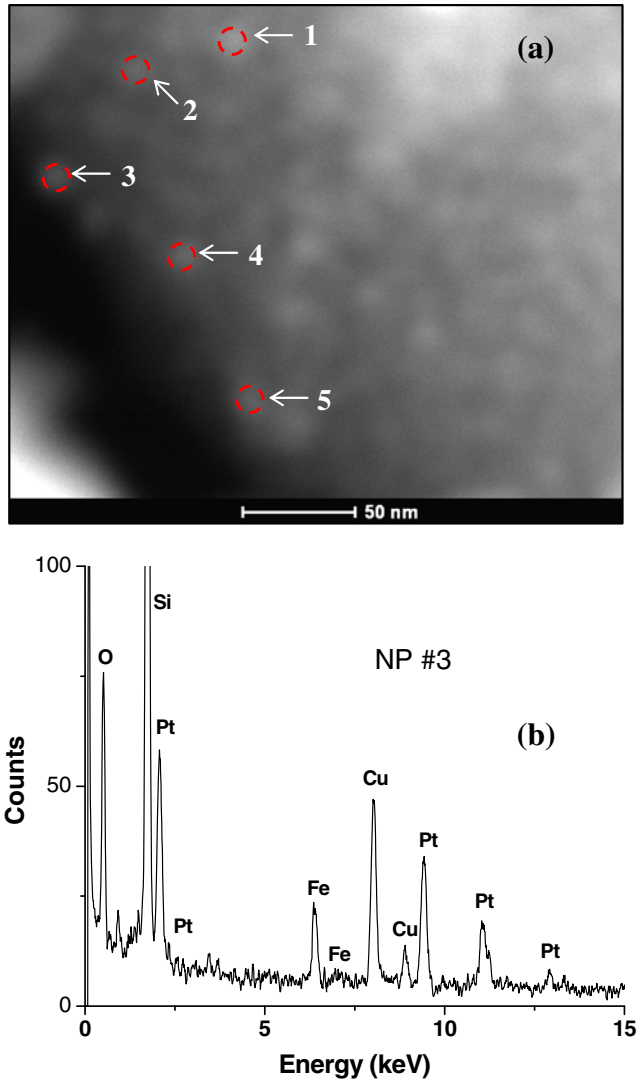

Figure 7. EDS measurements on single NP using nano-probe in STEM mode: (**a**) arbitrary chosen alloy NPs (marked by 1–5) are shown in HAADF–STEM image where nano-probe was focused and (**b**) a representative single NP EDX spectrum of NP#3 as marked in (**a**). Cu signals are from Cu grid.

Table 2. Quantitative elemental analysis on individual NPs (marked by 1–5 in figure 7a).

Alloy NPs	Atomic %	
	Fe	Pt
NP1	40·1	59·9
NP2	40·7	59·3
NP3	41·1	58·9
NP4	41·8	58·2
NP5	39·5	60·5

alloy composition. A representative EDX spectrum obtained from the NP marked as 3 is shown in figure 7b. The atomic ratios of Fe and Pt of each of these five NPs are presented in table 2. It has been observed that the atomic % values of Fe and Pt in all the individual NPs maintained quite homogeneous compositions (table 2) close to the expected value.

4. Conclusions

In this work the synthesis of fct $Fe_{0.42}Pt_{0.58}$ alloy NPs embedded SiO_2 films has been accomplished using the *in situ* hybrid sol–gel approach. In case of the pure Fe-doped film, the reduction of Fe ions was inhibited in SiO_2 matrix and heat treatment in reducing atmosphere caused crystallization of SiO_2 film matrix due to the presence of Fe ions. On the contrary, in case of the Fe/Pt co-doped film, the initially generated Pt NPs induced the reduction of Fe ions to Fe metal with the formation of Fe–Pt alloy NPs in amorphous SiO_2 film matrix. The SiO_2 matrix of the resulting fct Fe–Pt alloy NPs embedded film remained amorphous due to the absence of Fe ions. The fct Fe–Pt alloy NPs embedded SiO_2 films can find potential applications in magnetic storage devices and catalysis.

Acknowledgements

The Department of Science and Technology (DST), Govt. of India, is thankfully acknowledged for supporting this work under the Nano Mission programme (project # SR/S5/NM-17/2006).

References

Chen W, Kim J, Sun S and Chen S 2006 *Phys. Chem. Chem. Phys.* **8** 2779
Chen W, Kim J, Sun S and Chen S 2007a *Langmuir* **23** 11303
Chen W, Kim J, Xu L P, Sun S and Chen S 2007b *J. Phys. Chem.* **C111** 13452
Chou S W, Zhu C L, Neeleshwar S, Chen C L, Chen Y Y and Chen C C 2009 *Chem. Mater.* **21** 4955
Creighton J A and Eadon D G 1991 *J. Chem. Soc. Faraday Trans.* **87** 3881
De G and Rao C N R 2003 *J. Phys. Chem.* **B107** 13597
De G and Rao C N R 2005 *J. Mater. Chem.* **15** 891
Guglielme M and Maschio R D 1985 *Mater. Chem. Phys.* **13** 171
Howard L E M, Nguyen H L, Giblin S R, Tanner B K, Terry I, Hughes A K and Evans J S O 2005 *J. Am. Chem. Soc.* **127** 10140
Igarashi H, Fujino T, Zhu Y, Uchida H and Watanabe M 2001 *Phys. Chem. Chem. Phys.* **3** 306
Jana D, Dandapat A and De G 2009 *J. Phys. Chem.* **C113** 9101
Jitianu A, Crisan M, Meghea A, Rau I and Zaharescu M 2002 *J. Mater. Chem.* **12** 1401
Kiran P P, Bhaktha B N S, Rao D N and De G 2004 *J. Appl. Phys.* **96** 6717
Kong J Z, Gong Y P, Li X F, Li A D, Zang J L, Yan Q Y and Wu D 2011 *J. Mater. Chem.* **21** 5046
Lu M H, Song T, Zhou T J, Wang J P, Piramanayagam S N, Ma W W and Gong H 2004 *J. Appl. Phys.* **95** 6735
Mattei G, de Julian Fernandez C, Mazzoldi P, Sada C, De G, Battaglin G, Sangregorio C and Gatteschi D 2002 *Chem. Mater.* **14** 3440
Medda S K and De G 2009 *Ind. Eng. Chem. Res.* **48** 4326
Nanri H, Takeuchi N, Ishida S, Watanabe K and Wakamatsu M 1996 *J. Non-Cryst. Solids* **203** 375
Pal S and De G 2005 *Chem. Mater.* **17** 6161
Pal S and De G 2007 *J. Mater. Chem.* **17** 493
Pal S and De G 2008 *Phys. Chem. Chem. Phys.* **10** 4062
Pal S and De G 2009 *Mater. Res. Bull.* **44** 355
Pramanik S, Pal S, Bysakh S and De G 2011 *J. Nanopart. Res.* **13** 321
Sun S 2006 *Adv. Mater.* **18** 393
Sun S, Murray C B, Weller D, Folks L and Moser A 2000 *Science* **287** 1989
Wang H, Zhou M, Yang F, Wang J, Jiang Y, Wang Y, Wang H and Li Q 2009 *Chem. Mater.* **21** 404
Watanabe M, Zhu Y and Uchida H 2000 *J. Phys. Chem.* **B104** 1762
Wellons M S, Morris W H, Gai Z, Shen J, Bentley J, Wittig J E and Lukehart C M 2007 *Chem. Mater.* **19** 2483
Zeng H, Li J, Liu J P, Wang Z L and Sun S 2002 *Nature* **420** 395